2023 IEEE/ASME International Conference on Advanced Intelligent Mechatronics (AIM)
June 28-30, 2023. Seattle, Washington, USA

Simulation of Particle Motion on Rotating Cone Feeder for a Multihead Weigher Based on Dynamic Friction Modeling

Julia Isabel Hartmann, Michael Olbrich, Marcus Hamann, and Christoph Ament[1]

***Abstract*— This paper deals with particle motion on a cone-shaped feeder unit of an industrial multihead weigher, that distributes products through rotation. Thereby, rotational speed, rotational direction, and constraint-dependent friction substantially influence particle motion. Thus, particle motion is modeled considering dynamic friction and constraint forces for a viscoelastic case. Due to the cone-shape of the feeder, a specific kinematic model is proposed that comprises a differentiable restriction functions for calculating constraint forces. Afterwards, simulation results are tested against real data for a food application. Furthermore, application cases for the resulting model are proposed: The model can be incorporated into a digital twin environment of the weigher as well as used to generate simulation data for data-driven control algorithms.**

Keywords: Dynamic friction, constraint modeling, multihead weigher

I. INTRODUCTION

Food packaging industry requires product to be weighed, proportioned, and packaged to a predefined amount rapidly and precisely. For this purpose, food producers frequently employ multihead weighers (MHW) (see Fig. 1). The multihead weigher or combination scale is an industrial scale, that consists of multiple weighing heads and, thus, weighs several partial amounts simultaneously. Afterwards, a combination of partial amounts is formed that meets the predefined packaging amount precisely.

Thereby, a weighing cycle runs as follows:

i. Product is conveyed onto the cone-shaped rotary or vibratory feeder unit (cone feeder).
ii. The cone feeder conveys the product into radially outward leading dosing channels.
iii. The dosing channels move the product via vibration into the preliminary hoppers, that store the product until the weighing hopper underneath is available.
iv. The product is weighed in the weighing hopper and available for combination formation.
v. After determination of the hopper combination, the respective weighing hoppers are emptied and the product is lead over discharge chutes to a packaging machine.

*This work is part of the project "KiKO.BD-KI-Kombinationswaage mittels Big Data" of the programme "BayVFP Förderlinie Digitalisierung" of Bayerisches Staatsministerium für Wirtschaft, Landesentwicklung und Energie

[1] Julia Isabel Hartmann, Michael Olbrich, Marcus Hamann, and Christoph Ament are with Faculty of Applied Computer Science, University of Augsburg, 86159 Augsburg, Germany,
Julia Hartmann: julia.hartmann@uni-a.de;
Michael Olbrich: michael.olbrich@uni-a.de;
Marcus Hamann: marcus.hamann@uni-a.de;
Christoph Ament: christoph.ament@uni-a.de

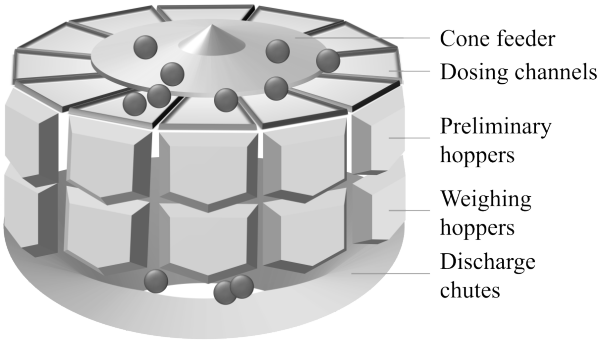

Fig. 1. Schematic illustration of a multihead weigher

Several aspects of the weighing process have already been addressed in literature: Since nominal hopper fill levels are often determined via rules of thumb, research seeks to obtain (near-) *optimal hopper set points* e.g. by means of Response Surface Methodology and a MHW machine simulator [2]. Thereby, costs for product surplus and shortage in a package have been considered. Furthermore, the MHW machine setup problem has been formalized and the performance of gradient-based, Brute Force, and random sampling optimization algorithms has been analyzed [3]. Moreover, different strategies for determining set points have been evaluated and optimized [8]. These strategies involve creating hoppers subgroups of equal set points with the set points being determined by a common average product amount and shifts in positive or negative direction.

Also, the *operation times of vibratory line feeders* have been optimized [14]. At that, operation times have been determined by (Weighted) Least Squares Method to supply product of varying shape and weight to the hoppers precisely in the amount specified by the set points.

Variability reduction and process optimization in the packaging process is also an issue in literature. Thereby, [16] and [1] measured the variability reduction in the MHW process by the percentage variability reduction index. Furthermore, the variability of different packaging strategies can be evaluated using a six-sigma approach [15]. In addition, modified control charts have been used to monitor and control the package weight for a packaging process optimized by a novel variability reducing packaging strategy [7].

Last, the *determination of the optimal hopper combination* is frequently addressed. Combination algorithms based on bit operation [13] and dynamic programming have been proposed by [11], [9], and [10]. Dynamic programming algorithms to find the optimal hopper combination for duplex

food packaging (simultaneous packaging of two packages) [11] [9], and mixture packaging of two elements [10] have been proposed. Furthermore, the performance of an enhanced dynamic programming algorithm for duplex packaging has been evaluated and compared to the quasi-duplex packaging process (packing two packages one after another without intermediate weighing) [9]. In addition, the combination problem has been stated as lexicographic, bi-criteria combinatorial optimization problem for two double-layered weigher configurations and solved via dynamic programming algorithms [12].

The methods used so far mainly investigate the optimum combination of the weights in the hoppers. However, a significant improvement could be achieved if a targeted weight distribution in the hoppers is already realized beforehand. This could be achieved by selectively dropping product from the cone feeder into the dosing channels, which requires knowledge about the motion of particles on a rotating feeder. To the best of the authors' knowledge, particle motion, including sticking and slipping, on a cone feeder in a MHW application or broader field has not yet been addressed in literature. However, some literature deals with particle motion and fluid flow in, on, or around rotating cones and disks as

- fluid flow around a rotating cone in still fluid [17],
- modeling of particles in a rotating flow for centrifugal separation mechanism [23],
- particle and gas dynamics in a rotating cone reactor [21],
- motion of granular material on rotating disk for bunker feeder [6] or screw conveyor [22],
- rolling of a ball on the inside surface of a rotating cone without slipping [5],
- particle separation inside a cone shaped rotating separator via rolling and sliding motion [4].

Nevertheless, these approaches are not suited for the problem at hand as they either involve a fluid flow or the main driving forces are others than adhesive and sliding friction. Therefore, an approach for modeling the movement of a particle on a rotating cone based on dynamic friction and constraint forces is proposed, that is especially suited, but not exclusively usable for a MHW. Thereby, the application case of a cone-shaped rotating feeder is novel and requires a new approach to continuously determine the constraint position and velocity.

This work is organized as follows: In section II the dynamic friction and constraint model for the particle motion on a rotating cone feeder is described including the determination of the constraint point. Next, section III presents the simulation and results thereof based on the model. Finally, some conclusions are drawn in section IV.

II. MODELING

To describe the particle motion accurately, a model must include both the impact and the adhesion and friction behavior. In both cases, constraint velocity is vital. A generalizable friction and constraint modeling approach has been described in [18] and [19], which will be adapted to the case of a MHW in the following.

For modeling, a particle is assumed to be described by its position $\mathbf{p} = [\mathrm{p_x}, \mathrm{p_y}, \mathrm{p_z}]^\mathrm{T}$ and velocity $\mathbf{v} = [\mathrm{v_x}, \mathrm{v_y}, \mathrm{v_z}]^\mathrm{T}$. The x-, y-, z-position of the particle is considered as generalized coordinates of the model.

$$\mathbf{q} = [\mathrm{q}_1, \mathrm{q}_2, \mathrm{q}_3]^\mathrm{T} = \mathbf{p} \tag{1}$$

Based on the generalized coordinates, a dynamic friction and constraint model is built. Thereby, the sticking and slipping of the particle results from friction; whereas, the constraint model ensures that the particle is only affected by friction when it touches the cone feeder.

At first, static friction is modeled. Then, the static model is expanded to a dynamic friction model by means of a low-pass filter. Afterwards, the constraint model is established and incorporated into the dynamic friction model.

For friction modeling, not the particle´s absolute velocity but the relative velocity between particle and cone feeder $\mathbf{v}_\mathrm{dif}$ is necessary. The velocity of the cone feeder $\mathbf{v}_\mathrm{p}$ at the particle position $\mathbf{q}$ for a given rotational speed ω is

$$\mathbf{v}_\mathrm{p}(\mathbf{q}) = \omega \times \mathbf{q}\,. \tag{2}$$

Thus, the *relative velocity* $\mathbf{v}_\mathrm{dif}$, its direction $\mathbf{e}_\mathrm{v}$, and value v are given by

$$\mathbf{v}_\mathrm{dif}(\mathbf{q}, \dot{\mathbf{q}}) = \dot{\mathbf{q}} - \mathbf{v}_\mathrm{p}(\mathbf{q}) \tag{3}$$

$$\mathbf{e}_\mathrm{v}(\mathbf{q}, \dot{\mathbf{q}}) = -\frac{\mathbf{v}_\mathrm{dif}(\mathbf{q}, \dot{\mathbf{q}})}{|\mathbf{v}_\mathrm{dif}(\mathbf{q}, \dot{\mathbf{q}})| + \varepsilon} \tag{4}$$

$$\mathrm{v} = |\mathbf{v}_\mathrm{dif}(\mathbf{q}, \dot{\mathbf{q}})| \tag{5}$$

with the parameter ε to ensure numeric stability by avoiding zero division [20].

A. Static friction model

The *static friction force* $\mathbf{Q}_\mathrm{s}$ consists of viscous $\mathbf{F}_\mathrm{V}$, Coulomb $\mathbf{F}_\mathrm{C}$, and Stribeck friction $\mathbf{F}_\mathrm{S}$.

$$\mathbf{Q}_\mathrm{s}(\mathbf{q}, \dot{\mathbf{q}}) = \mathbf{F}_\mathrm{V}(\mathbf{q}, \dot{\mathbf{q}}) + \mathbf{F}_\mathrm{C}(\mathbf{q}, \dot{\mathbf{q}}) + \mathbf{F}_\mathrm{S}(\mathbf{q}, \dot{\mathbf{q}}) \tag{6}$$

The functions for viscous, Coulomb, and Stribeck friction force are defined analogously to [18].

Viscous friction force behaves proportionally to the relative velocity with the damping parameter d.

$$\mathbf{F}_\mathrm{V}(\mathbf{q}, \dot{\mathbf{q}}) = \mathrm{d}\,\mathrm{v}\,\mathbf{e}_\mathrm{v}(\mathbf{q}, \dot{\mathbf{q}}) \tag{7}$$

Coulomb friction force depends on the sliding friction coefficient μ_C, normal force $\mathrm{F}_\perp$, and parameter $\mathrm{v_C}$, that defines the slope of the approximated sliding friction curve during zero crossing. The tanh-function is favored over the sign function to express the direction dependency of the Coulomb friction and avoid the non-differentiable properties of the sign function by a smoothed transition [18].

$$\mathbf{F}_\mathrm{C}(\mathbf{q}, \dot{\mathbf{q}}) = \mu_\mathrm{C}\,\mathrm{F}_\perp \tanh\left(\frac{\mathrm{v}}{\mathrm{v_C}}\right) \mathbf{e}_\mathrm{v}(\mathbf{q}, \dot{\mathbf{q}}) \tag{8}$$

Stribeck friction force depends on the adhesive friction coefficient μ_S and the parameter $\hat{v}_S$, where $\hat{v}_S$ defines the velocity that would result in the maximum adhesive force.

$$\mathbf{F}_S(\mathbf{q},\dot{\mathbf{q}}) = \mathbf{F}_S^{\Delta}\,\frac{v}{\hat{v}_S}\,e^{\frac{1}{2}-\frac{1}{2}\left(\frac{v}{\hat{v}_S}\right)^2}\,\mathbf{e}_v(\mathbf{q},\dot{\mathbf{q}}) \tag{9}$$

with

$$\mathbf{F}_S^{\Delta} = \left(\mu_S - \mu_C \tanh\left(\frac{\hat{v}_S}{v_C}\right)\right)\mathbf{F}_\perp - d\,\hat{v}_S\,. \tag{10}$$

Based on the static friction $\mathbf{Q}_s$ and the weight force $\mathbf{F}_g = [0,\,0,\,-m\,g]^T$, Newton´s second law can be applied to obtain the following differential equation for particle motion

$$\ddot{\mathbf{q}} = \frac{1}{m}(\mathbf{Q}_s(\mathbf{q},\dot{\mathbf{q}}) + \mathbf{F}_g)\,. \tag{11}$$

B. Dynamic friction model

The static model does not adequately represent the dynamic friction effects and results in a zero force during standstill. This is due to a lack of hysteresis and memory effect, which can be avoided by an extension to a dynamic friction model using a linear parameter-varying low-pass filter At that, static friction force $\mathbf{Q}_s$ is delayed and the delayed force $\mathbf{Q}_d$ is applied to the system. [18]
Thus, (11) adapts to

$$\ddot{\mathbf{q}} = \frac{1}{m}(\mathbf{Q}_d(\mathbf{q},\dot{\mathbf{q}}) + \mathbf{F}_g(\mathbf{q},\dot{\mathbf{q}}))\,. \tag{12}$$

This requires the introduction of $\mathbf{Q}_d$ as a new system state. The following first order differential equation describes the dynamics of $\mathbf{Q}_d$ with T_F as time constant of the low-pass filter.

$$\dot{\mathbf{Q}}_d(\mathbf{q},\dot{\mathbf{q}}) = \frac{a(\dot{\mathbf{q}})}{T_F}\,(\mathbf{Q}_s(\mathbf{q},\dot{\mathbf{q}}) - \mathbf{Q}_d(\mathbf{q},\dot{\mathbf{q}})) \tag{13}$$

with

$$a(\dot{\mathbf{q}}) = 1 - e^{-\left(\frac{\mathbf{v}_{diff}(\mathbf{q},\dot{\mathbf{q}})}{\dot{\mathbf{q}}_F}\right)^2}\,. \tag{14}$$

The parameter $a(\dot{\mathbf{q}})$ adapts the filter dynamics to the different relative velocities and, thus, to the system dynamics [18].

C. Constraint model

To ensure that particle motion is only influenced by friction when the particle is in contact with the cone feeder, a constraint model is established. Furthermore, the constraint model allows to represent the collision and bouncing of the particle on the cone feeder. Thereby, the general constraint modeling approach is based on [19] and the interested reader is referred to [19] for further details.

As the surface of the cone feeder represents the constraint, with which the particle collides, at first, a novel type of constraint distance function for the cone feeder is proposed. Afterwards, the proposed constraint distance function is used for the dynamic constraint and friction model.

1) Cone feeder constraint distance function: The constraint distance function $s_\perp(\mathbf{q})$ calculates the distance between the constraint (cone feeder surface) and the center of mass of the particle based on its position $\mathbf{q}$. The challenge of this application is the nonlinear, three dimensional motion of the particle with respect to the cone feeder.

For modeling the constraint distance function, the cone feeder is assumed to be a straight cone with height h, radius r, and a circular base. For sake of simplicity, the attached second cone, that is depicted in Fig. 1, is neglected and the cone base center $\mathbf{O}$ is the origin of the considered coordinate system. The simplified cone is depicted in Fig. 2. Additionally, a condensed form of writing the formulas without dependencies on generalized coordinates is used. In the following, uppercase letters denote points and lowercase letters their respective position vectors.

For the constraint distance function $s_\perp(\mathbf{q})$, the collision point $\mathbf{C}$ between particle and cone must be calculated continuously via an analytical function. $\mathbf{C}$ corresponds to the momentary collision point between particle and cone, if the particle is in free fall without the influence of external forces other than gravity. At first, the position $\mathbf{q}$ of the particle is projected onto the cone base to obtain a hypothetical intersection $\mathbf{C}_b$ with the cone base.

$$\vec{c}_b = \begin{pmatrix} q_1 \\ q_2 \\ 0 \end{pmatrix} \tag{15}$$

Then, a straight line is placed through the cone base center $\mathbf{O} = (0,0,0)$ and the hypothetical intersection $\mathbf{C}_b$ to determine the intersection $\mathbf{B}$ with the boundary of the cone base. This results in the following equation

$$\vec{x}_{base} = \vec{o} + \lambda_b(\vec{c}_b - \vec{o}) = \lambda_b \cdot \vec{c}_b\,. \tag{16}$$

As the boundary of the cone base has the distance r to the center $\mathbf{O}$, it follows

$$|\vec{x}_{base}| = \lambda_b\sqrt{q_1^2+q_2^2} \stackrel{!}{=} r \Longleftrightarrow \lambda_b^* = \frac{r}{\sqrt{q_1^2+q_2^2}}\,. \tag{17}$$

Thus, the intersection with the boundary $\mathbf{B}$ is given by

$$\vec{b} = \lambda_b^* \cdot \vec{c}_b\,. \tag{18}$$

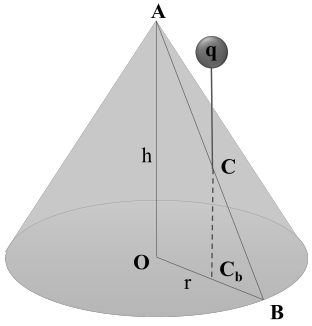

Fig. 2. Simplified cone for determination of the constraint distance function

To obtain the collision point $\mathbf{C} = (q_1, q_2, c_z)$, the line equation for the cone surface line from the point $\mathbf{B}$ to the tip $\mathbf{A} = (0,0,h)$ must be established as follows

$$\vec{c} = \vec{a} + \lambda(\vec{b} - \vec{a}). \tag{19}$$

Considering (19) line by line, a system of three equations with each equation representing a dimension results.

$$c_x = a_x + \lambda(b_x - a_x) \Longleftrightarrow c_x = \lambda b_x \tag{20}$$
$$c_y = a_y + \lambda(b_y - a_y) \Longleftrightarrow c_y = \lambda b_y \tag{21}$$
$$c_z = a_z + \lambda(b_z - a_z) \Longleftrightarrow c_z = h + \lambda(b_z - h) \tag{22}$$

To obtain the coordinates of the collision point $\mathbf{C}$, the system of equations must be solved. Since the x- and y-position of $\mathbf{C}$ are given by q_1 and q_2, a system of equations with two unknowns (λ and c_z) remains.

$$q_1 = \lambda b_x \tag{23}$$
$$q_2 = \lambda b_y \tag{24}$$
$$c_z = h + \lambda(b_z - h) \tag{25}$$

Solving the equation system leads to

$$\lambda^* = \frac{q_1}{b_x} = \frac{q_1}{\frac{r}{\sqrt{q_1^2+q_2^2}} \cdot c_{b,x}} = \frac{q_1}{\frac{r}{\sqrt{q_1^2+q_2^2}} \cdot q_1} = \frac{\sqrt{q_1^2+q_2^2}}{r} \tag{26}$$

which can be used to calculate the z-coordinate of the collision point

$$c_z = h + \lambda^*(b_z - h) = h\left(1 - \frac{\sqrt{q_1^2+q_2^2}}{r}\right). \tag{27}$$

Based on the collision point the distance $s_\perp$ between particle and cone can be calculated as

$$s_\perp = q_3 - c_z. \tag{28}$$

Further, the relative velocity between particle and constraint is given by

$$\frac{d}{dt} s_\perp = v_\perp = \dot{q}_3 + \frac{h}{r}\left(\frac{q_1\dot{q}_1 + q_2\dot{q}_2}{\sqrt{q_1^2+q_2^2}}\right). \tag{29}$$

2) Power-based restriction function: According to [19], mathematically the power of a constraint can be represented as a restriction function R. The restriction function depends on the distance $s_\perp$ between the particle and constraint and the relative velocity $v_\perp$ between both.

$$R(s_\perp(\mathbf{q}), v_\perp(\mathbf{q}, \dot{\mathbf{q}})) = R_a(s_\perp(\mathbf{q}))\, R_p(v_\perp(\mathbf{q}, \dot{\mathbf{q}})) \tag{30}$$

The restriction function consists of an *activation function* R_a and *constraint-specific power function* R_p.

Based on the distance $s_\perp$ between object and constraint the activation function R_a identifies constraints. Also, R_a determines the intensity of interaction between constraint and particle as well as the activity state of the constraint. For elastic particles with an outer radius s_0 and compression radius $s_c < s_0$ the continuous activation function is defined as

$$R_a(s_\perp(\mathbf{q})) = \frac{1 - \tanh(r_t(s_\perp(\mathbf{q}) - r_c))}{2} \in (0,1) \tag{31}$$

with the transition coefficient r_t that describes the rigidity of the particle

$$r_t = \frac{2}{s_0 - s_c} \operatorname{artanh}(r_a) \tag{32}$$

and the constraint offset r_c that refers to the geometry of the particle

$$r_c = \frac{s_0 + s_c}{2}. \tag{33}$$

For $R_a(s_\perp) \to 0$ there is no contact between particle and constraint and, thus, the constraint is inactive. For $R_a(s_\perp) \to 1$ a contact exists and the interaction between particle and constraint is at its maximum.

The constraint-specific power function defines the energy dissipation for a certain relative velocity between particle and constraint based on a dissipation coefficient r_d and the maximum force r_f the constraint can provide.

$$R_p(v_\perp(\mathbf{q}, \dot{\mathbf{q}})) = \left(\frac{v_\perp(\mathbf{q}, \dot{\mathbf{q}})}{2} - \frac{\log(\cosh(r_d\, v_\perp(\mathbf{q}, \dot{\mathbf{q}})))}{2 r_d}\right) r_f \tag{34}$$

D. Combined dynamic friction and constraint model

To merge constraint and friction model, the normal force $F_\perp$ between particle and constraint must be calculated. It is obtained by the partial derivative of the restriction function R with respect to the relative velocity $v_\perp$. In addition, to transform the effective direction of the constraint resistance force F_c and, thus, the normal force $F_\perp$ in the direction of the generalized variables $\mathbf{q}$, the relative velocity must be partially derived with respect to the generalized velocities $\dot{\mathbf{q}}$

$$\begin{aligned} F_\perp((\mathbf{q}, \dot{\mathbf{q}}) &= \frac{\partial R(\mathbf{q}, \dot{\mathbf{q}})}{\partial v_\perp(\mathbf{q}, \dot{\mathbf{q}})} \frac{\partial v_\perp(\mathbf{q}, \dot{\mathbf{q}})}{\partial \dot{\mathbf{q}}} \\ &= R_a(s_\perp(\mathbf{q}))\left(\frac{1 - \tanh(r_d v_\perp(\mathbf{q}, \dot{\mathbf{q}}))}{2}\right) r_f \vec{\mathbf{e}}_{F_c} \\ &= R_a(s_\perp(\mathbf{q}))\, F_c(v_\perp(\mathbf{q}, \dot{\mathbf{q}}))\, \vec{\mathbf{e}}_{F_c} \end{aligned} \tag{35}$$

with

$$\vec{\mathbf{e}}_{F_c} = \frac{\partial v_\perp(\mathbf{q}, \dot{\mathbf{q}})}{\partial \dot{\mathbf{q}}} = \begin{pmatrix} \frac{h}{r} \frac{q_1}{\sqrt{q_1^2+q_2^2}} \\ \frac{h}{r} \frac{q_2}{\sqrt{q_1^2+q_2^2}} \\ 1 \end{pmatrix}. \tag{36}$$

$F_\perp(\mathbf{q}, \dot{\mathbf{q}})$ is then inserted into the static friction force $\mathbf{Q}_s$ in place of $F_\perp$ corrected with the factor $\frac{1}{r_f}$. This leads to the constraint-specific static friction force $\mathbf{Q}_s^c$. For viscous friction an exception applies. As $\mathbf{F}_V$ does not depend on the normal force $F_\perp$, $\mathbf{F}_V$ is just multiplied by the activation function R_a to generate the dependency between the occurrence of a contact to the constraint and viscous friction force.

Furthermore, the dynamic friction force and its dynamics are influenced by the constraint modeling as follows

$$\dot{\mathbf{Q}}_d^c(\mathbf{q}, \dot{\mathbf{q}}) = \frac{a(\dot{\mathbf{q}})}{T_F}\left(\mathbf{Q}_s^c(\mathbf{q}, \dot{\mathbf{q}}) - \mathbf{Q}_d^c(\mathbf{q}, \dot{\mathbf{q}})\right). \tag{37}$$

Last, the normal force $F_\perp$ must be incorporated into the differential equation for particle motion as follows

$$\ddot{\mathbf{q}} = \frac{1}{m}(\mathbf{Q}_d^c(\mathbf{q},\dot{\mathbf{q}}) + \mathbf{F}_g(\mathbf{q},\dot{\mathbf{q}}) + F_\perp((\mathbf{q},\dot{\mathbf{q}}))\,. \tag{38}$$

III. SIMULATION AND RESULTS

Real data from a food industry application is used for simulation. In this application, the MHW weighs raw meat pieces and proportions them to a predefined package size. To achieve the package size most accurately, meat is pre-proportioned via the preliminary hoppers. Thereby, the cone feeder indirectly determines the fill levels of the preliminary hoppers by ejecting meat into specific dosing channels. In this application, especially product properties are a challenge, namely the varying shape, unit weights, and adhesive behavior with other products and the metal cone feeder. To loosen adhering meat and convey it to the dosing channels, the cone feeder rotates clockwise and counterclockwise according to a predefined pattern.

Data on five meat pieces sticking and slipping on the cone feeder are extracted from a video of this process using image recognition. Table I shows an overview of the start position, angle when leaving the feeder, and dosing channel the meat piece is conveyed to for these five meat pieces. Thereby, meat pieces 1, 2, and 3 are moved by a clockwise rotation, 4 and 5 by a counterclockwise rotation. Moreover, meat piece 4 represents a single piece of meat lying on the cone feeder and adhering to it. In contrast, meat pieces 1, 2, 3, and 5 are located on the cone feeder together with several others, partially overlapping meat pieces resulting in interactions between these meat pieces.

By means of the proposed model, the trajectory of a meat piece and its exit point from the cone feeder is simulated for a given start position and speed curve. The simulation parameters are summarized in table II. All meat pieces are assumed to start at the height of the cone feeder as the actual start height cannot be determined from the 2D video. For the adhesive and sliding friction coefficient, high values are assumed to represent the stickiness of the meat. In addition,

TABLE I
PRODUCT DATA

Sample	Start position [m]	Exit angle	Exit channel
1	$\begin{pmatrix} 0.11 \\ -0.01 \\ 0.03 \end{pmatrix}$	69.5 °	2
2	$\begin{pmatrix} -0.10 \\ -0.01 \\ 0.03 \end{pmatrix}$	63.5 °	2
3	$\begin{pmatrix} 0.08 \\ -0.13 \\ 0.03 \end{pmatrix}$	93.6 °	1
4	$\begin{pmatrix} -0.07 \\ 0.04 \\ 0.03 \end{pmatrix}$	(147.4 °)	(13)
5	$\begin{pmatrix} 0.14 \\ 0.06 \\ 0.03 \end{pmatrix}$	115.2 °	14

TABLE II
SIMULATION DATA

ε	0.0000001
d_i mit i = 1...5	(225 135 750 750 30)
μ_c	0.85
v_c	0.00005 $\frac{m}{s}$
μ_s	0.99
v_s	0.1 $\frac{m}{s}$
m	0.125 kg
T_F	0.0003 s
$\dot{q}_{IF}$	0.0001 $\frac{m}{s}$
g	9.81 $\frac{m}{s^2}$
s_0	0.025 m
s_c	0.5 s_0
r_a	0.99
r_d	120 $\frac{s}{m}$
r_f	120 N
Cone diameter	0.45 m
Cone tilt	7.5 °
Dosing channels	14

the meat pieces are assumed to behave viscoelastically with a maximum thickness compression of 50%. The cone feeder is assumed to be rigid and not breakable by falling meat pieces. MATLAB R 2022a is used for the numerical simulation with the data shown in table II.

The results of the simulation are summarized in table III and Fig. 3. The simulation results show a good approximation of the real trajectories with small errors in the exit angles for the more common case of meat being ejected from the cone feeder (1, 2, 3, 5). The case of meat sticking to the feeder (5) can be modeled as well but the error regarding the end position is significantly larger. Considering the real data from the video, this difference might occur due to the different setting of a single meat piece lying on the feeder without any interaction with other meat pieces that possibly could push it down. To solve this issue, a larger experiment for identifying the model parameters and an expansion of the model by particle interactions is advised.

IV. CONCLUSIONS

The presented model is a first step to approximate particle motion on a cone-shaped rotating feeder and we were able to confirm experimental results for the most part. The proposed model lays the foundation to control product distribution in the multihead weighing process. On this basis, we will expand the model for collision dynamics between multiple particles and develop product-specific models. Beyond that, we will design a controller for the cone feeder to realize

TABLE III
SIMULATION RESULTS

Sample	1	2	3	4	5
Exit angle	70.0 °	62.0 °	93.8 °	(287.4 °)	119.0 °
Error	0.5 °	-1.5 °	0.2 °	(140.0 °)	3.8 °
Exit channel	2	2	1	(10)	14

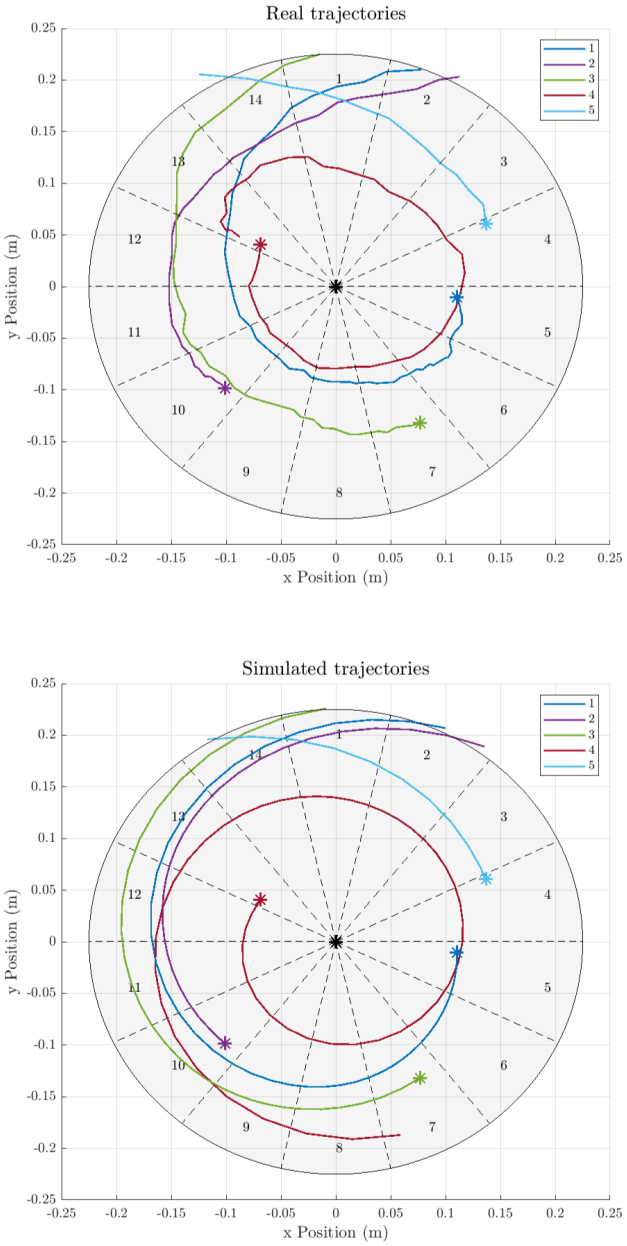

Fig. 3. Real vs. simulated particle motion trajectories

a targeted and more precise product distribution in the weighing hoppers.

Applications for the developed model are the incorporation of the model into a digital twin environment or data generation for data-driven control algorithms such as Reinforcement Learning Control.

References

[1] J. J. Barreiro, C. González, and M. Salicrú. Optimization of multiweighing packing proceedings. *Top*, 6(1):37–44, 1998.

[2] Alessia Beretta and Quirico Semeraro. On a rsm approach to the multihead weigher configuration. In *Volume 1: Advanced Computational Mechanics; Advanced Simulation-Based Engineering Sciences; Virtual and Augmented Reality; Applied Solid Mechanics and Material Processing; Dynamical Systems and Control*, pages 225–233. American Society of Mechanical Engineers, 2012.

[3] Alessia Beretta, Quirico Semeraro, and Enrique Del Castillo. On the multihead weigher machine setup problem. *Packaging Technology and Science*, 29(3):175–188, 2016.

[4] E. M. Beunder, K. A. van Olst, and P. C. Rem. Shape separation on a rotating cone. *International Journal of Mineral Processing*, 67(1-4):145–160, 2002.

[5] Alexey V. Borisov, Tatiana B. Ivanova, Alexander A. Kilin, and Ivan S. Mamaev. Nonholonomic rolling of a ball on the surface of a rotating cone. *Nonlinear Dynamics*, 97(2):1635–1648, 2019.

[6] S. Yu. Borovikov, L. A. Tarasova, and O. A. Troshkin. Movement of a granular material on a rotating disk in a bunker-spreader system. *Chemical and Petroleum Engineering*, 38(3/4):124–127, 2002.

[7] J. Carlos García-Díaz and Alexander Pulido-Rojano. Monitoring and control of the multihead weighing process through a modified control chart. *DYNA*, 84(200):135–142, 2017.

[8] J. Carlos Garcia-Diaz and Alexander D. Pulido-Rojano. Performance analysis and optimisation of new strategies for the setup of a multihead weighing process. *European J. of Industrial Engineering*, 14(1):58–84, 2020.

[9] Shinji Imahori, Yoshiyuki Karuno, Rena Nishizaki, and Yui Yoshimoto. Duplex and quasi-duplex operations in automated food packing systems. In *2012 IEEE/SICE International Symposium on System Integration (SII)*, pages 810–815. IEEE, 2012.

[10] Shinji Imahori, Yoshiyuki Karuno, and Kenju Tateishi. Dynamic programming algorithms for producing food mixture packages by automatic combination weighers. *Journal of Advanced Mechanical Design, Systems, and Manufacturing*, 8(5):JAMDSM0065–JAMDSM0065, 2014.

[11] Shinji Imahori, Yoshiyuki Karuno, and Yui Yoshimoto. Dynamic programming algorithms for duplex food packing problems. In *2010 8th IEEE International Conference on Industrial Informatics*, pages 857–862. IEEE, 2010.

[12] Yoshiyuki Karuno, Hiroshi Nagamochi, and Xiaoming Wang. Optimization problems and algorithms in double-layered food packing systems. *Journal of Advanced Mechanical Design, Systems, and Manufacturing*, 4(3):605–615, 2010.

[13] J. N. Keraita and K. H. Kim. A weighing algorithm for multihead weighers. *International Journal of Precision Engineering and Manufacturing*, 8(1):21–26, 2007.

[14] James N. Keraita and Kyo-Hyoung Kim. A study on the optimum scheme for determination of operation time of line feeders in automatic combination weighers. *Journal of Mechanical Science and Technology*, 20(10):1567–1575, 2006.

[15] Alexander D. Pulido-Rojano and J. Carlos Garcia Diaz. Optimization of multihead weighing process using the taguchi loss function, 2014.

[16] M. Salicrú, C. González, and J. J. Barreiro. Variability reduction with multiweighing proceedings. *Top*, 4(2):319–329, 1996.

[17] Antonio Segalini and Simone Camarri. Flow induced by a rotating cone: Base flow and convective stability analysis. *Physical Review Fluids*, 4(8), 2019.

[18] T. Specker, M. Buchholz, and K. Dietmayer. A new approach of dynamic friction modelling for simulation and observation. *IFAC Proceedings Volumes*, 47(3):4523–4528, 2014.

[19] Thomas Specker, Michael Buchholz, and Klaus Dietmayer. Dynamical modeling of constraints with friction in mechanical systems. *IFAC-PapersOnLine*, 48(1):514–519, 2015.

[20] Thomas Specker. *Leistungsbasierte Modellierung dynamischer Reib- und Kontaktprozesse in mechanischen Systemen*. Dissertation, Universität Ulm, Ulm, 08.01.2016.

[21] B. M. Wagenaar, J.A.M. Kuipers, and W.P.M. van Swaaij. Particle dynamics and gas-phase hydrodynamics in a rotating cone reactor. *Chemical Engineering Science*, 49(7):927–936, 1994.

[22] Fangping Ye, Yu Li, Jiquan Hu, and Kaikai Chen. Investigation of particle dynamics in a disc rotating device by means of experiments and numerical simulations using dem. *JOURNAL OF CHEMICAL ENGINEERING OF JAPAN*, 51(8):631–640, 2018.

[23] Jiangang Zhang, Xitong Zhang, Ningning Wang, Haihu Liu, and Guang Xi. Lattice boltzmann modeling of particle dynamics in rotating coordinate system. *Physics of Fluids*, 33(12):123316, 2021.